

Adaptive hybrid density functionals

Danish Khan,^{1,2} Alastair James Arthur Price,^{1,3} Maximilian L. Ach,^{4,5}
Olivier Trottier,^{3,4} and O. Anatole von Lilienfeld^{1,2,3,4,6,7,8,*}

¹*Chemical Physics Theory Group, Department of Chemistry,
University of Toronto, St. George Campus, Toronto, ON, Canada*

²*Vector Institute for Artificial Intelligence, Toronto, ON, Canada*

³*Acceleration Consortium, University of Toronto, Toronto, ON, Canada*

⁴*Department of Physics, University of Toronto, St. George Campus, Toronto, ON, Canada*

⁵*Department of Physics, Ludwig-Maximilians-Universität, Munich, Germany*

⁶*Department of Materials Science and Engineering,*

University of Toronto, St. George Campus, Toronto, ON, Canada

⁷*Machine Learning Group, Technische Universität Berlin, 10587 Berlin, Germany*

⁸*Berlin Institute for the Foundations of Learning and Data, 10587 Berlin, Germany*

Exact exchange and correlation contributions are known to crucially affect electronic states, which in turn govern covalent bond formation and breaking in chemical species. Empirically averaging the exact exchange admixture and the amount of correlation over configurational and compositional degrees of freedom, hybrid density functional approximations (DFAs) have been widely successful, yet have fallen short to reach explicitly correlated high level quantum chemistry accuracy in general. Using quantum machine learning, we have adapted hybrid DFAs by generating optimal admixture ratios of exact exchange or of correlation “on the fly”, specifically for any chemical compound. Adaptive exchange in the PBE0 hybrid DFA yields atomization energies sufficiently accurate to effectively cure the infamous spin gap problem in DFT, and also improves electron densities, and HOMO-LUMO gaps in organic molecules. Using adaptive PBE0, we revised the entire QM9 data set presenting more accurate quantum properties that include, on average, stronger covalent binding, larger band-gaps, more localized electron densities, and slightly larger dipole-moments. Adaptive PBE correlation (in conjunction with 100% HF exchange) also affords much improved atomization energies, and even enables covalent bond dissociation.

I. INTRODUCTION

Current key challenges necessitate substantial progress in inverse design of novel materials and chemicals, paving the way for a more sustainable future.^{1,2} Quantum mechanics underpins the ability to predict electronic, optical, and thermal properties with high fidelity, essential for designing materials with specific functionalities.^{3,4} Unfortunately, while universal and general in principle, due to its computational complexity, numerically solving the many-body electronic Schrödinger equation has remained an outstanding challenge for all but the simplest systems. Even the most recent and promising machine learning based efforts,^{5–7} still rely heavily on considerable training data needs, require the optimization of billions of regression weights, or struggle to efficiently extrapolate across chemical space. By contrast, density functional theory (DFT) is a formally ex-

act quantum method but unfortunately the exact density functional is only known to exist, with no prescription to be found.⁸ Nevertheless, it enables the definition and parametrization of density functional approximations (DFAs) which stand out in terms as the most viable trade-off between predictive power and computational cost, effectively turning it into the most useful workhorse for computational materials and molecular discovery,⁹ also thanks to its high degree of reproducibility¹⁰. Many approximations to the exact functional have been made over the years^{11–13} and while currently the most reasonable tool for an impressive array of compound classes and properties, common DFAs still struggle to reach the accuracy seen by other post-HF methods^{11,14,15}. A large number of such shortcomings stem from what is known as self-interaction error (SIE), which arises from the Hartree energy term that includes the interaction of the electron with itself¹³. SIE manifests in a number of well known ways, from the poor performance for band gap energies,^{16–18} to the example of DFT’s failure in accurately predicting how molecules form or break apart,

* anatole.vonlilienfeld@utoronto.ca

e.g. the dissociation limit of the H_2^+ ion.^{13,19–21} A related challenge for DFT is the prediction of spin gaps, critical to the understanding of reactivity and magnetism, which can be both quantitatively and qualitatively incorrect.²²

Rooted rigorously in adiabatic connection²³, some of these issues are reduced or mitigated by hybrid functionals that blend in HF exchange (also referred to as exact exchange) with the DFA exchange energy,

$$E_X^{\text{hybrid}} = aE_X^{\text{HF}} + (1 - a)E_X^{\text{DFA}}, \quad (1)$$

where a is the mixing parameter, varying between 0 and 1. Global hybrids were originally parameterized for general thermochemistry, and contain a fixed amount of exact exchange, typically around 20–25%. Although legacy hybrid functionals such as B3LYP²⁴ or PBE0^{25,26} represented significant advancements for energetics and electron densities, they are not a panacea: More recently proposed DFAs were noted to sacrifice the accuracy of calculated electron densities for improved energy predictions^{11,27}. Common hybrid based DFA parameterizations attempt to find the average optimum of a single universal admixture ratio to all chemistries and properties. However, Langreth and Perdew observed already in 1975²⁸ that non uniform systems can be modeled extremely well when tuning the exact exchange. The system dependency of optimal exchange admixture ratios has also been noted by Johnson¹⁵. For example, even the most recent functionals do not reach chemical accuracy when it comes to reaction energies, barrier heights, thermochemistry, or systems with large self-interaction errors²⁹. The same authors also point out that, at the expense of being specific to each system, optimal exchange admixture ratios can drastically reduce the error. Optimal admixture ratios are also a persistent issue for molecular crystals, where increasing amounts of HF exchange can be required to recover the experimentally observed structures as the lowest energy on the crystal energy landscape.^{30,31} Within another large scale study, the importance of exact exchange admixture for correctly reproducing the correct high-spin low-spin ordering in first and second row transition metal complexes was noted.³² But also the quality of hybrid DFA based molecular adsorption energies on transition metal oxide surfaces was shown to be strongly admixture dependent.³³ Pasquarello and co-workers demonstrated dramatic improvements of band-gap predictions in insulators and semiconductors by tuning the amount of exact exchange³⁴. Also, Mewes, Grimme, and co-workers recently high-lighted the potential of tuning range-separated hybrid functionals³⁵.

Last but not least, varying amounts of exact exchange in molybdenum carbide systems resulted in direct reordering of spin-energies.²²

Based on these observations, we hypothesize the optimal admixture ratio a_{opt} to be a system specific scalar label with sufficient smoothness characteristics and which approaches zero DFA error with respect to a trust-worthy high level electronic structure treatment. As long as the hypothesis holds, we note that system specific optimal admixture ratios will not violate energy conservation as they simply reproduce the reference level of theory which can be assumed to conserve energy. Below, we present overwhelming numerical evidence in support of our hypothesis, and demonstrate that we can efficiently regress and estimate a_{opt} throughout chemical compound space using suitable QML models^{36,37} (figure 1). Based on the MBDF representation³⁸, our KRR based QML ansatz is highly data efficient and light weight (no more than 3'000 regression weights) in mapping directly from the $4N-6$ internal degrees of freedom that define the electronic system to one scalar parameter in the Kohn-Sham Hamiltonian that only varies mildly in system changes. This differs fundamentally from previously published ML based efforts aimed at improving DFAs which are significantly more challenged since they map the full electron density information, and varying during the self-consistent field cycles, to energy expectation values which are very sensitive and strongly varying labels. In particular, in 2017 a machine learning model of the Hohenberg-Kohn map from external potential to electron density to energy was proposed³⁹. In 2020, neural network models were shown to successfully map electron density based descriptors to energies and forces^{40,41}, while the more recent DM21 functional by Kirkpatrick et al⁴² accounts for crucial additional constraints on fractional electron number and spin by learning the map from the spin indexed electron charge, gradient, kinetic energy, and two range separated HF densities to the exchange-correlation energy. Concurrently, Margraf and Reuters presented a pure kernel ridge regression functional model predicting electron correlation using the HF density as an input⁴³, similar other orbital based representations^{44,45}. The Δ -ML⁴⁶ based functional by Bogojeski et al⁴⁷ also maps electron density to an energy (enabling force predictions). While more light weight and also more scalable, through use of ‘Amon’-based fragments⁴⁸, by virtue of its embedding within standard KS-DFT SCFs, our adaptive hybrid functional generates at least the same wealth of information (orbitals, eigenvalues, densities, energies) as all the other

ML based functionals mentioned. Furthermore, it can conveniently be integrated in widely spread DFT codes which would facilitate its adaptation by a large international community of users, estimated to publish at least 30'000 papers each year⁴⁹.

In the following we first demonstrate how our adaptive version of the PBE0 functional improves upon all commonly used DFAs for obtaining qualitatively and quantitatively correct singlet-triplet spin gaps in carbenes. We then show simultaneous improvements in other properties, on top of atomization energies, namely in electron densities and frontier orbital gaps, indicating that the method does not sacrifice accuracy of one observable in favour of the other¹¹. Finally, we revise the entire QM9 dataset⁵⁰, a molecular benchmark containing hybrid DFT quantum properties of over 130'000 small to medium sized organic molecules, generated within the exhaustive molecular graph enumeration efforts by Raymond and co-workers⁵¹, that has emerged as a widely used benchmark set for novel QML methods. Using our adaptive PBE0 functional trained on Coupled Cluster Singles Doubles perturbative Triples (CCSD(T)), we report properties with an estimated quality that is vastly superior to the original.

II. RESULTS

A. Spin gaps

Following the procedure described in the Methods section, a training set of optimal exact exchange percentage, a_{opt} , values was obtained using the singlet and triplet state energies at MRCISD+Q⁵²⁻⁵⁴ level of theory reported for ~ 3000 carbenes within the QMspin⁵⁵ dataset. All geometries used correspond to the restricted open shell B3LYP/def2-TZVP⁵⁶ optimized triplet state structures in QMspin. The adiabatic spin-gap is then defined as the difference between the singlet and triplet state energies ($E_s - E_t$) of the molecule in the same geometry (which is the same as the atomization energy difference). Two separate ML models were trained to predict the $a_{\text{opt}}^s, a_{\text{opt}}^t$ values which recover corresponding atomization energies for any carbene molecule. Learning curves indicate that our models reach close to 1% prediction error of a_{opt} for $\sim 2'800$ carbene molecules used in training (see Fig.12 SI). Figure 2A shows the distribution of the $a_{\text{opt}}^s, a_{\text{opt}}^t$ values predicted with the largest model. Compared to closed shell QM9 counterparts (see meth-

Level of Theory	MAE [kcal/mol]	# of wrong signs
aPBE0 (Opt.)	0.14	0
aPBE0 (ML)	3.89	2
B3LYP	5.63	11
MP2	6.64	14
ω B97XD	7.63	10
M06-2X	8.25	7
PBE0	10.15	61
PBE	11.06	37
BLYP	16.08	13
r ² SCAN	17.59	61

Table I. Mean absolute adiabatic spin gap ($E_s - E_t$) errors to MRCISD+Q for 111 particularly challenging (for default PBE0) carbenes from the QMspin⁵⁵ dataset. aPBE0 (Opt.) refers to the PBE0 functional employing the optimal HF exchange fraction for all molecules found via optimization while aPBE0 (ML) uses the HF exchange fraction predicted by our ML model trained on 2800 carbenes. For all DFT calculations we used the restricted open shell method while for MP2 we used the unrestricted method. The cc-pVTZ basis set was employed in all calculations.

ods and figure 1), these values are significantly shifted towards larger HF exchange ratios with mean values of around 95 and 105 % for a_{opt}^s and a_{opt}^t , respectively. The two values also show a strong correlation ($R_2 = 0.93$) as can be seen from the inset in 2A with a_{opt}^t being larger in almost all cases (99.3%) likely due to larger delocalization and self-interaction errors in the triplet state. Figure 2B shows the improvement of the spin gap ($\Delta E_{s-t} = E_s - E_t$) error obtained via (restricted open shell) DFT calculations performed with the aPBE0 functional as a function of the training set size. This test set was chosen as a subset of carbenes where default PBE0 calculations give even qualitatively wrong results for the spin gap ΔE_{s-t} predicting incorrect ordering of the two structures. One of the reasons behind this shortcoming of hybrid DFT is the difference in delocalization and SI errors²². The qualitative failures of PBE0 is cured by aPBE0 method which uses optimum HF exchange values for both states, as predicted by their respective ML models. From figure 2(B) it can be seen that training on just 100 structures, the aPBE0 functional already reduces the number of incorrect orderings from 50 to 6, while also reducing the quantitative (mean) error by more than half. Since this is a general issue for KS-DFT, we

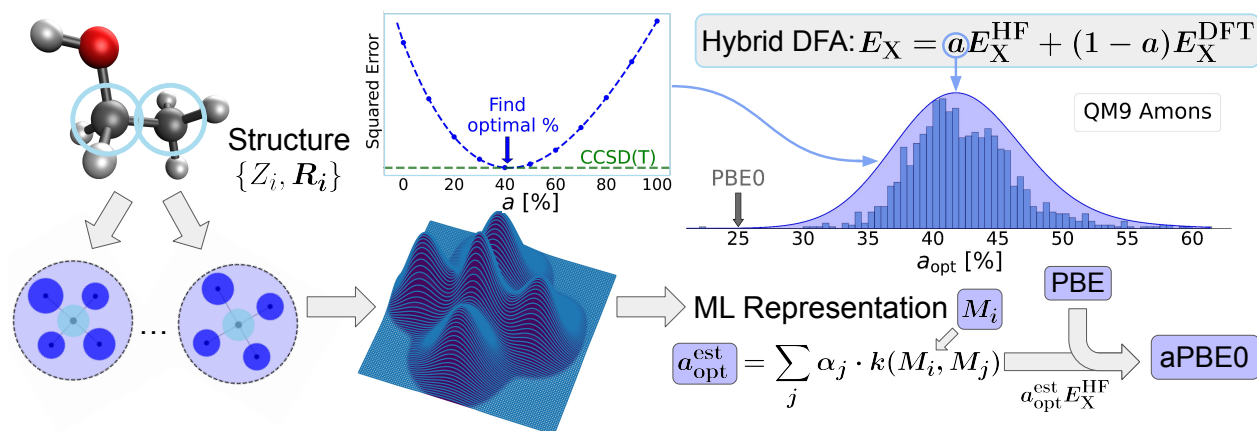


Figure 1. Workflow for the adaptive PBE0 (aPBE0) functional: A structure’s nuclear charges and coordinates (which define the external potential in the electronic Hamiltonian) map to a suitable representation which, thanks to the kernel trick, enables linear regression using non-linear feature similarity measures³⁷. The optimal Hartree-Fock (HF) exchange ratio a_{opt} to be mixed with the PBE functional in a hybrid DFT calculation can then be predicted by the ML model for any system of interest. Training set of optimal admixture ratios are obtained by fitting the DFT atomization energy to a reference value obtained from a high level calculation such as CCSD(T).

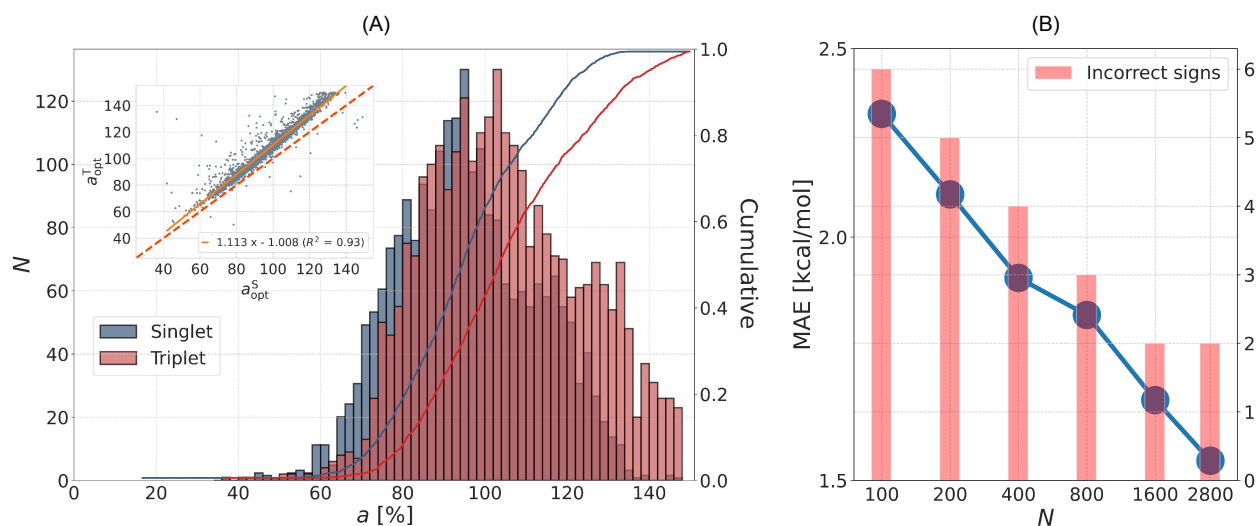


Figure 2. (A) Distribution of optimal HF exchange % values for singlet (a_{opt}^s) and triplet (a_{opt}^t) carbene states found by optimizing to MRCISD+Q atomization energies in the QMspin dataset⁵⁵. (B) aPBE0 performance curve showing carbene singlet-triplet mean absolute (MAE) adiabatic spin gap ($E_s - E_t$) errors and number of incorrect orderings (bar plot) compared to MRCISD+Q values for 50 particularly challenging out-of-sample carbenes (not part of training) from the QMspin⁵⁵ dataset as a function of training set size N . The MAE for non-adaptive PBE0 for this set is 4.8 kcal/mol, with all 50 signs being incorrect.

benchmark some of the most commonly used functionals in Table 2 on a test set of carbenes where PBE0 shows the largest errors. It can be seen that inclusion of HF

exchange improves the performance of the DFT methods as the hybrid functionals outperform the most commonly used GGAs/meta-GGAs and closely match/outperform

the wavefunction based 2nd order perturbation theory (MP2) method. The aPBE0 (ML) functional which uses the optimum exact exchange values predicted by our ML models outperforms all the other functionals and MP2 as well while still retaining the cost of PBE0. Furthermore, we found that an optimum HF exchange value exists for both electronic states and for all the tested structures. This can be seen from the aPBE0 (Opt.) method in table 2 which employs the optimum a_{opt}^s , a_{opt}^t values for all structures and provides nearly exact predictions in all cases. Hence, with larger training sets the ML model will improve, and the aPBE0 based estimates can be expected to reach the exact ones, a trend that is also on display for the performance curve in figure 2(B). A lower offset on the performance curve can likely be achieved by making one of the other more accurate DFAs adaptive or using a double hybrid functional with both the exchange and correlation mixture ratios adapted to the system.

B. Energies, densities, HOMO-LUMO gap

The spin gap values obtained from the aPBE0 functional approach the exact value since the functional minimizes the error to the exact atomization energies of each respective spin state of the system. Correspondingly, Figure 3 shows the improvement in singlet atomization energy estimates using aPBE0 (compared to CCSD(T)) when using a_{opt} predicted for 50 random closed shell molecules from the QM9 dataset⁵⁰ containing 9 heavy atoms, and for which Quantum Monte Carlo (QMC) data were obtained previously⁵⁷. Corresponding learning curves indicate that our models reach less than 0.5% prediction error of a_{opt} for ~ 1100 QM9 amon molecules used in training (see Fig. 10 in the SI). Furthermore, Fig. 11 (in the SI) shows that the prediction errors for the b_{opt} values in the aPBE0c functional are even lower ($\sim 0.25\%$) suggesting possibly larger improvements when fixing the exchange part to HF exchange and varying the ratio of PBE correlation instead.

Turning to the electron density, we compare corresponding changes to CCSD densities (integrated error shown as an inset in figure 3). The a_{opt} values for these molecules were predicted by the ML model trained on a set of 1169 amon⁴⁸ based small organic molecular fragments containing not more than 5 heavy atoms from Ref.⁵⁷ (figures 1, 6). The training a_{opt} values were always obtained by minimizing the atomization energy error to

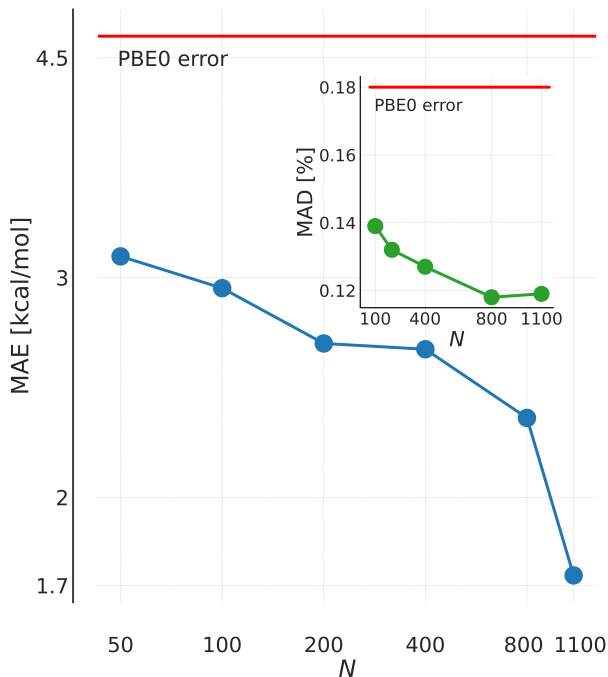


Figure 3. aPBE0 performance curve showing atomization energy errors compared to CCSD(T) values for the 50 organic molecules from the QM9 dataset⁵⁰ discussed in Ref.⁵⁷ as a function of training set size N . Inset shows the corresponding change in % mean absolute deviation (MAD), $\sqrt{\int d\mathbf{r}(\rho_{\text{aPBE0}} - \rho_{\text{CCSD}})^2} / \int d\mathbf{r}\rho_{\text{CCSD}}^2$, to CCSD electron densities. The training set consists of the 1169 amon⁴⁸ based small organic molecular fragments from Ref.⁵⁷ containing not more than 5 heavy atoms.

CCSD(T). Our model shows good transferability as the predicted values for these larger molecules already lead to improved atomization energies and electron densities with as little training as 50 amons compared to default PBE0. Table 2 shows the average prediction errors for atomization energy on this test set with other popular functionals and MP2. The commonly known trend for energies, and similar to the one noted for spin gaps, is observed with hybrid functionals performing better than the GGAs PBE⁵⁸ and BLYP^{59,60}. The popular meta-GGA $r^2\text{SCAN}$ ^{61,62} performs well on this set with errors close to the best performing hybrid functionals, the hybrid meta-GGA M06-2X⁶³ and the long range corrected hybrid ωB97XD ⁶⁴. We again found that an optimum HF exchange ratio existed for all molecules which provided

Level of Theory	MAE [kcal/mol]
aPBE0 (Opt.)	0.02
aPBE0 (ML)	1.32
M06-2X	3.61
ω B97XD	3.63
r ² SCAN	3.82
PBE0	4.68
MP2	5.76
B3LYP	5.94
PBE	8.38
BLYP	11.48

Table II. Mean Absolute atomization energy Errors (MAE) compared to CCSD(T) values for the 50 organic molecules from the QM9 dataset⁵⁰ discussed in Ref.⁵⁷ using different DFAs and MP2. aPBE0 (Opt.) refers to the PBE0 functional employing the optimal HF exchange fraction for all molecules found via optimization while aPBE0 (ML) uses the HF exchange fraction predicted by our ML model trained on the 1169 QM9 amons from Ref.⁵⁷ (see Fig. 3). Errors for all methods were shifted via linear regression to account for differences in free atom energy errors.

nearly exact (CCSD(T)) atomization energies for these molecules with the aPBE0 (Opt.) functional providing a near zero error on average. The aPBE0 (ML) functional using the HF exchange ratios predicted by our trained ML model reached close to spectroscopic accuracy (~ 1 kcal/mol) outperforming all the other methods which shows that hybrid DFAs can be pushed close to the accuracy of high level explicitly correlated wavefunction methods by adapting the functional to the system of interest.

We further used our ML model trained on QM9 fragments to predict the optimal exchange ratios for 100 random small organic molecules from the QM7b^{36,65} dataset. This was done to compare the changes in molecular orbital (MO) eigenvalues as the optimal HF exchange ratio is varied. Table 3 shows mean absolute errors for HOMO-LUMO gaps compared to the reference single particle Green’s function and screened Coulomb interaction (GW)⁶⁶ approach values reported in the dataset. It can be seen that our model shows good transferability with the aPBE0 HOMO-LUMO gap errors being reduced by more than a factor of 3 when compared to default PBE0. It also outperforms all other functionals except M06-2X which is a more expensive meta-GGA hybrid functional. This is especially promis-

Level of Theory	MAE [eV]
M06-2X	0.670
aPBE0 (ML)	0.857
ω B97XD	1.082
LC- ω PBE	1.366
B3LYP	3.278
PBE0	3.524
r ² SCAN	4.262
PBE	5.006
BLYP	5.072

Table III. HOMO-LUMO gap errors compared to GW eigenvalues for 100 molecules from the QM7b dataset⁶⁵. aPBE0 (ML) uses the HF exchange fraction predicted by our ML model trained on the 1169 QM9 amons from Ref.⁵⁷.

ing since the optimum labels for our ML model were always found by optimizing the atomization energy without any information about the electron density or MO eigenvalues being incorporated. Hence, we believe that a higher rung of Perdew’s ladder can be defined with adaptive functionals while retaining the computational cost of a lower rung. Further improvements might be seen by making long-range corrected/meta-GGA hybrids such as ω B97XD/M06-2X adaptive which already provide appreciably better predictions than PBE0 in all our tests. Finally, we mention here briefly that dissociation curves are also improved by our functionals, albeit with differing magnitudes, as shown by the H2+ (Fig. 8) and H2 (Fig. 7) dissociation curves in the SI. In both cases we found a pole for the a_{opt} values as a function of the bond distance while the b_{opt} values show smooth behaviour. This indicates that the aPBE0c functional is likely more well suited for PES exploration and AIMD.

C. Revised QM9 dataset

Our adaptive functionals lead to improved physical properties at the same DFT computational cost. Over the past decade statistical models have emerged as promising (and highly efficient) alternative methods which can bypass solving the electronic Schrodinger equation⁶⁷ lowering the computational cost significantly. Since the accuracy of all statistical models is bounded by the quality of the reference data, we believe that adaptive DFT functionals can lead to the improvement of all ML models by

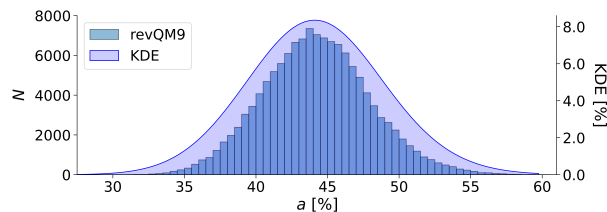


Figure 4. ML-predicted a_{opt} values for 130k QM9 molecules after training on 1169 QM9 amons from Ref.⁵⁷. These values were subsequently used to perform aPBE0 calculations to generate the revQM9 dataset.

providing higher quality reference training data for which DFT has been the primary source⁹. Since figure 3 and table 2 indicate that our ML model can accurately predict the optimal exchange ratios for molecules from the QM9 dataset, we demonstrate this use case by providing a revised version of QM9 which is perhaps the most widely used and benchmarked quantum chemistry dataset for developing ML models.

The HF exchange ratio to be used with the aPBE0 functional for each molecule was predicted by our ML model trained on the CCSD(T) based labels for the same 1169 QM9 amons from Ref.⁵⁷ (figure 3). The predicted HF exchange ratios for the 130k molecules are shown in figure 4. These values show a nearly perfect normal distribution centered at 44% exact exchange with a standard deviation of 3.7. Out of all, 8625 molecules required more than 50% exact exchange and only 6 molecules required less than 30% exact exchange. Following this we performed single point DFT calculations with the aPBE0 functional and the cc-pVTZ basis set for the ~130k QM9 molecules using the PySCF 2.4.0 package⁶⁸. The calculations consumed ~15 node days parallelized over multiple in-house nodes (36 core 4.8GHz Intel Xeon W9-3475X/24 GB RTX 4090/1 TB DDR5 ECC RAM). For each molecule in this revised QM9 (revQM9) dataset we provide total energies, atomization energies, MO energies, dipole moments and density matrices. Figure 5 shows the distribution of atomization energies, HOMO-LUMO gaps and dipole moment norms for the original QM9 and our revQM9 datasets. The MAE between the 130k atomization energies of the QM9 and revQM9 datasets is 16.82 kcal/mol. This larger difference compared to table 2 is likely due to our use of the larger (triple zeta) and more balanced cc-pVTZ basis set compared to the 6-31G(2df,p) (double zeta) basis set used in

the original QM9 dataset. For validation we performed CCSD(T)/cc-pVTZ calculations for a subset of 41 randomly chosen molecules and obtained atomization energy MAEs of 15.86 kcal/mol (QM9) and 1.98 kcal/mol (revQM9) respectively. For HOMO-LUMO gaps we found an average difference of -1.95 eV (revQM9 - QM9) between the two datasets. Comparison with table 3 and the fact that HOMO-LUMO gaps are underestimated by KS-DFT¹⁵ would suggest that this is likely an average improvement of ~ 2 eV per molecule. We note the striking similarity of the average gap (~7 eV) and average optimal admixture values (~44 %) between the organic molecules in revQM9 and the insulating solids reported in Ref.³⁴.

For dipole moments, hybrid functionals such as B3LYP and PBE0 have been shown to be highly accurate compared to higher level wavefunction based methods^{69,70} such as CCSD. The size of the basis set has been shown to have a larger effect on dipole moments and polarizabilities⁶⁹. The mean difference (revQM9 - QM9) between the dipole moment norm values is 0.18 Debye which is likely due to the better basis set employed in our calculations.

Finally, we also provide density matrices for all molecules as these were not included in the original QM9 dataset and are also improved by our aPBE0 functional. On the test set of 50 QM9 molecules in table 2, we obtained % MAD to CCSD densities of 0.11 (aPBE0), 0.18 (PBE0) and 0.25 (B3LYP) with the cc-pVTZ basis set in all cases.

III. CONCLUSIONS AND FUTURE WORK

This work successfully exploited the hypothesis that optimal exact exchange admixture a_{opt} or optimal correlation amount b_{opt} in hybrid DFAs dramatically reduce prediction errors. Numerical evidence reported in the literature, as well as our own calculations are fully consistent with this hypothesis. Our machine learning models also indicate that a_{opt} and b_{opt} are sufficiently smooth in chemical compound space to enable efficient regression and effective generalization with negligible computational overhead. Integration of ‘on-the-fly’ machine learning based predictions of a_{opt} within adaptive hybrid DFT functional (such as aPBE0) and use for ~ 3000 carbenes in singlet and triplet states results in statistics that would suggest that the well known spin-gap prediction problem of common DFAs can be resolved. aPBE0

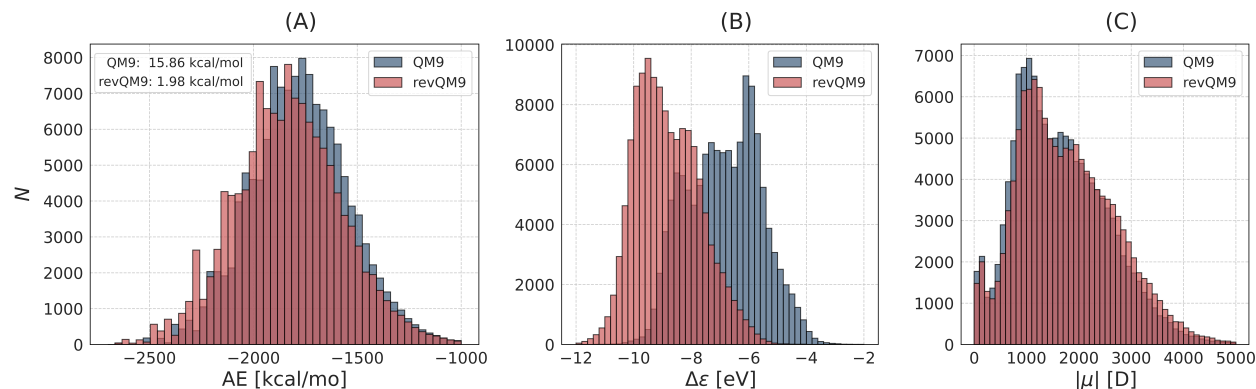


Figure 5. (A) Atomization energy [kcal/mol] (B) HOMO-LUMO gap [eV] (C) Dipole moment norm (Debye) distribution plots for the original QM9 and the revised QM9 (revQM9) datasets. Inset in figure A shows mean absolute errors to CCSD(T)/cc-pVTZ atomization energies on a random subset of 41 molecules for the two datasets.

based estimates of atomization energies, electron densities, and HOMO-LUMO gaps of thousands of small organic molecules were also shown to improve significantly. Encouraged by the performance of aPBE0, we have revised the entire QM9 data set in order to present much improved estimates of energies, orbital energies, dipole moments, and electron density matrices. Using the amon data set, bPBE0 was shown to be amenable to machine learning based predictions. With respect to changes in atomic configurations, however, a_{opt} exhibits discontinuous behavior while b_{opt} does not. Smoothness being a requisite for machine learning, this finding would suggest that b_{opt} is a more promising target for machine learning all purpose adaptive hybrid DFAs.

Overall, our adaptive hybrid DFAs are shown to outperform popular functionals for relative energies, such as singlet-triplet spin state gaps or atomization energies, and binding curves; and significant improvements for other properties such as molecular orbital eigenvalues and electron densities have also been observed. The improvement of other properties (that were not part of training) highlights the power of this method and is reminiscent of what is known as ‘foundational model’ within the machine learning community. We also note that adaptive exchange and correlation are also amenable to combinations with other popular post-SCF corrections, such as the many-body dispersion⁷¹, Johnson’s exchange-hole dipole moment⁷², or Grimme’s D3⁷³ method enabling the treatment of non-covalent van der Waals interactions.

While this work has focused on the exact exchange and correlation admixture ratio within the global hybrid GGA PBE0 functional due to its simplicity, it has not escaped our attention that the same strategy could be applied to any hybrid functional. Furthermore, we expect even larger improvements with smaller training needs when using adaptive meta-GGA/range-separated hybrids or double hybrids with adaptive correlation as well. More generally speaking, we believe that there is much merit in adaptifying model Hamiltonian parameters, as also corroborated by promising results within semi-empirical quantum chemistry⁷⁴ or tight binding DFT^{75,76}. Similar but more recent contributions include the ML- ω PBE by Lin and co-workers^{77,78} and the ML based prediction of element specific atom centred correction parameters by Di Labio and co-workers⁷⁹.

Further refinements to the methodology could also be made in the spirit of Ref.⁴², namely by imposing additional exact constraints and adding other terms to the loss function, such as density errors. Future work will deal with these avenues, and possible limitations, for example due to the fixed functional form of given approximate Hamiltonians (even though adaptive force-field parameters of simple Stillinger Weber potentials indicate impressive predictive power when ‘learnt-on-the-fly’⁸⁰), or due to discontinuities of adaptive parameters in certain linear combinations of configurational and compositional degrees of freedom. In particular, such smoothness would imply the applicability of this approach towards the nav-

igation of chemical compound space as well as *ab initio* molecular dynamics simulations.

IV. COMPUTATIONAL METHODS

A. Adaptive hybrids

Hybrid exchange-correlation DFAs mix a portion of HF exchange energy (E_X^{HF})

$$E_X^{\text{HF}} = -\frac{1}{2} \sum_{\sigma} \sum_{ij} \iint \varphi_{i\sigma}^*(\mathbf{r}) \varphi_{j\sigma}^*(\mathbf{r}') \frac{1}{|\mathbf{r} - \mathbf{r}'|} \varphi_{i\sigma}(\mathbf{r}') \varphi_{j\sigma}(\mathbf{r}) d\mathbf{r} d\mathbf{r}', \quad (2)$$

where $\varphi_{i\sigma}$ are spin orbitals; with the DFA exchange (E_X^{DFA}) and correlation (E_C^{DFA}) energy^{24,81}

$$E_{\text{XC}}^{\text{hybrid}} = aE_X^{\text{HF}} + (1-a)E_X^{\text{DFA}} + bE_C^{\text{DFA}} \quad (3)$$

with the admixture ratio of exchange a and correlation b being respectively close to 25% and 100% for popular hybrid functionals such as PBE0^{25,58} and B3LYP²⁴. In our work we assume the optimal admixture ratios to adapt, i.e. to be system specific in the sense that it becomes a function of the external potential and the electronic state, which can be machine learnt and predicted on the fly for new, out-of-sample systems. We dub this the adaptive PBE0 functional (aPBE0) for varying the balance of HF and PBE exchange,

$$E_{\text{xc}}^{\text{aPBE0}} = a(\{Z_I, \mathbf{R}_I\}_I, S_j) E_X^{\text{HF}} \quad (4)$$

$$+ (1-a(\{Z_I, \mathbf{R}_I\}_I, S_j)) E_X^{\text{PBE}} + bE_C^{\text{PBE}} \quad (5)$$

where $\{Z_I, \mathbf{R}_I\}_I$ denotes the set of nuclear charges and coordinates respectively, S_j denotes the spin state of the system and the DFT exchange-correlation energies come from the PBE functional.

Conversely, when varying correlation, we set a to 100% and predict the amount of PBE correlation that is blended in. More specifically,

$$E_{\text{xc}}^{\text{aPBE0c}} = E_X^{\text{HF}} + b(\{Z_I, \mathbf{R}_I\}_I, S_j) E_C^{\text{PBE}} \quad (6)$$

The correlation term in this functional now corrects for the errors in the kinetic energy, Coulombic repulsion and HF exchange in the Kohn-Sham non-interacting system.

B. Optimization

The optimal admixture ratios a_{opt} or b_{opt} were always found by minimizing the squared error of the atomization energy E_{atm} with respect to a high level reference

$$a_{\text{opt}} = \arg \min_a (E_{\text{atm}}^{\text{aPBE0}}(a) - E_{\text{atm}}^{\text{Ref.}})^2 \quad (7)$$

where the reference values $E_{\text{atm}}^{\text{Ref.}}$ correspond to either CCSD(T)⁸²⁻⁸⁵ or Multi-Reference Configuration Interaction Singles Doubles with Davidson correction (MRCISD+Q)^{52-54,86,87} values in our work. The aPBE0 atomization energies are defined as

$$E_{\text{atm.}}^{\text{aPBE0}}(a) = E^{\text{aPBE0}}(a) - \sum_i \varepsilon_i^{\text{aPBE0}}(a) \quad (8)$$

where $E^{\text{aPBE0}}(a)$ denotes the total energy and $\varepsilon_i^{\text{aPBE0}}(a)$ denotes the aPBE0 free atom energy of atom i using admixture ratio a . Unless stated otherwise, the cc-pVTZ⁸⁸ basis set was employed and the PySCF 2.4.0^{68,89,90} package was used for all DFT and (all electron) CCSD(T) calculations. For optimization we performed a simple grid scan by obtaining $E_{\text{atm.}}^{\text{aPBE0}}(a)$ at evenly spaced values of a between 0 and 100%. The squared error to the reference (eq. (7)) was then interpolated using a quartic polynomial fit to obtain the minimum which we found to be nearly exact in all cases. Following this procedure we performed CCSD(T) and PBE0 calculations for 1169 small organic molecules with upto 5 heavy atoms⁴⁸ obtained from the QM9 dataset^{50,57} to find the optimal admixture ratios for all molecules. A few examples of these are shown in figure 6A with appreciably different a_{opt} values. The distribution plot of these 1169 a_{opt} values is shown in the workflow figure 1 with a nearly perfect normal distribution around 42% HF exchange. Throughout our work we found an a_{opt} value to exist which reduces the atomization energy error to nearly 0 for all cases. The mean absolute error for these 1169 atomization energies is reduced from 3.46 to 0.02 kcal/mol by using the optimal HF exchange percentage with the PBE0 functional for all molecules. A similar procedure was followed to obtain a_{opt} for ~3000 carbenes in singlet and triplet state from the QMSpin dataset⁵⁵. All calculations were performed using the Restricted Open shell Kohn-Sham (ROKS) method. Separate a_{opt} were obtained for singlet and triplet state structures via optimization to MRCISD+Q atomization energies. Figure 6B shows the optimization fits for a few carbenes in the singlet and triplet states while 2A shows the distribution of $a_{\text{opt}}^s, a_{\text{opt}}^t$ for the ~3000 carbenes.

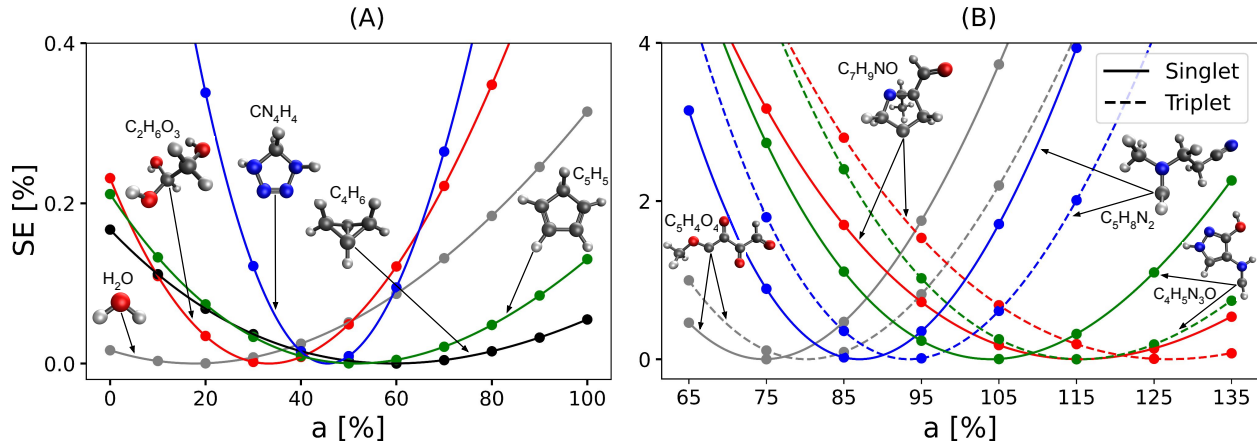


Figure 6. Squared atomization energy errors of PBE0 calculations with variable HF exchange percentage for (A) amons from the QM9 dataset compared to CCSD(T) and (B) carbenes from the QMspin dataset compared to MRCISD+Q. A grid search was conducted and the optimal exact exchange ratio was found via a quartic polynomial fit. The procedure was repeated and labels were generated for all molecules used during training of the machine learning models.

C. Machine Learning

This can be done efficiently by using high-level quantum reference training data for atoms-in-molecules based fragments (amons)⁴⁸ due to their small size. Subsequent training and predictions are done on the product of a_{opt} and the number of electrons in the system which makes it an extensive property and the QML model highly transferable to larger systems thanks to local partitioning schemes^{48,57,91,92}.

With the generated a_{opt} values as training data, ML models were developed to predict the optimal HF exchange values to be used alongside the PBE functional for systems of interest. The ML model used throughout this work is Kernel Ridge Regression^{93–95} (KRR) due to its high robustness and simplicity, which has been used extensively with QML models^{57,67,96,97}. The optimal HF exchange values for the query molecule, a_{opt}^q , can be obtained as weighted sums of similarity measures to all molecules in the training set

$$a_{\text{opt}}^q = \sum_J^{N_{\text{train}}} \alpha_J k(\mathbf{M}^q, \mathbf{M}_J) \quad (9)$$

where α_j are the regression weights, \mathbf{M} are molecular representation feature vectors which depend only on the set of nuclear charges and coordinates, and $k(\cdot, \cdot)$ denotes a kernel function acting as a similarity measure. The ker-

nel function primarily used in our work is the screened local Gaussian kernel

$$k(\mathbf{M}_I, \mathbf{M}_J) = \sum_{\mu \in I} \sum_{\nu \in J} \delta_{Z_\mu, Z_\nu} \exp\left(-\frac{\|\mathbf{x}_{I\mu} - \mathbf{x}_{J\nu}\|_2^2}{2\sigma^2}\right) \quad (10)$$

where $\mathbf{x}_{I\mu}$ denotes the representation vector of atom a within molecule I and δ_{Z_μ, Z_ν} denotes a Kronecker Delta over the nuclear charges Z_μ, Z_ν which restricts the similarity measurement between atoms of the same chemical element⁹⁸. The regression weights α are obtained from the set of training labels $\mathbf{y}^{\text{train}}$ via the following equation

$$\alpha = (\mathbf{K} + \lambda \cdot \mathbf{I})^{-1} \mathbf{y}^{\text{train}} \quad (11)$$

where \mathbf{K} is the kernel matrix of the training set and λ is a regularization parameter. The form of the kernel function in eq. (10) partitions the system into atomic contributions. This local partitioning is vital to the transferability of ML models to larger systems and has been successfully applied to the learning of size extensive properties^{48,99,100}. However, such partitioning is not suitable to the learning of intensive properties such as the HF exchange admixture ratio, a_{opt} , in our case⁶⁷. To circumvent this issue we follow the recipe of Chen et al⁹¹ to instead learn the product of the intensive property with the extensive number of particles. More specifically, we

predict the product of a_{opt} with the total number of electrons (N_e) with an atomic ML model. The label y_{opt} to be learned and predicted then becomes

$$y_{\text{opt}} = N_e a_{\text{opt}} \quad (12)$$

The representation used for generating atomic feature vectors for the ML model in our work is an extended version of the Many-Body Distribution Functionals (MBDF) representation³⁸. The reason for this choice is its compact size, leading to fast predictions, but nevertheless high predictive power. Briefly, MBDF uses functionals of two- and three-body distribution functionals as atomic feature vector components:

$$F_{2\text{body}}^{nm}[i] = \int_0^\infty dr g_n(r) \partial_r^m \rho_i(r), \quad (13)$$

$$\rho_i(r) = \sum_j^M Z_j \mathcal{N}(R_{ij}, \sigma_r)$$

$$F_{3\text{body}}^{nm}[i] = \int_0^\pi d\theta g_n(\theta) \partial_\theta^m \rho_i(\theta), \quad (14)$$

$$\rho_i(\theta) = \sum_{jk}^M \frac{(Z_j Z_k)^{\frac{1}{2}} \mathcal{N}(\theta_{ijk}, \sigma_\theta)}{(R_{ij} R_{jk} R_{ik})^2}$$

where \mathcal{N} denotes a normalized Gaussian, Z_j denotes atomic number of atom j , R_{ij} , θ_{ijk} denote interatomic dis-

tances and angles respectively and g_n are suitable weighting functions similar to 2, 3-body interaction potentials.

DATA AND CODE AVAILABILITY

Scripts and a trained model for predicting the optimum exact exchange admixture ratio with the aPBE0 functional along with generated CCSD(T) training data are available at <https://github.com/dkhan42/aPBE0>. The revised QM9 (revQM9) dataset calculated with the aPBE0 functional and cc-pVTZ basis set is publicly available at <https://doi.org/10.5281/zenodo.10689884>.

ACKNOWLEDGEMENTS

D.Khan acknowledges discussions with B. Huang. O.A.v.L. has received funding from the European Research Council (ERC) under the European Union’s Horizon 2020 research and innovation programme (grant agreement No. 772834). This research was undertaken thanks in part to funding provided to the University of Toronto’s Acceleration Consortium from the Canada First Research Excellence Fund, grant number: CFREF-2022-00042. O.A.v.L. has received support as the Ed Clark Chair of Advanced Materials and as a Canada CIFAR AI Chair.

-
- ¹ A. Zunger, *Nature Reviews Chemistry* **2**, 0121 (2018).
² B. Sanchez-Lengeling and A. Aspuru-Guzik, *Science* **361**, 360 (2018).
³ G. Ceder, *Science* **280**, 1099 (1998).
⁴ A. Franceschetti and A. Zunger, *Nature* **402**, 60 (1999).
⁵ G. Carleo and M. Troyer, *Science* **355**, 602 (2017).
⁶ D. Pfau, J. S. Spencer, A. G. Matthews, and W. M. C. Foulkes, *Physical Review Research* **2**, 033429 (2020).
⁷ J. Hermann, Z. Schätzle, and F. Noé, *Nature Chemistry* **12**, 891 (2020).
⁸ A. E. Mattsson, *Science* **298**, 759 (2002).
⁹ B. Huang, G. F. von Rudorff, and O. A. von Lilienfeld, *Science* **381**, 170 (2023).
¹⁰ K. Lejaeghere, G. Bihlmayer, T. Björkman, P. Blaha, S. Blügel, V. Blum, D. Caliste, I. E. Castelli, S. J. Clark, A. Dal Corso, *et al.*, *Science* **351**, aad3000 (2016).
¹¹ M. G. Medvedev, I. S. Bushmarinov, J. Sun, J. P. Perdew, and K. A. Lyssenko, *Science* **355**, 49 (2017).
¹² K. Burke, *J. Chem. Phys.* **136**, 150901 (2012).
¹³ A. D. Becke, *The Journal of chemical physics* **140** (2014).
¹⁴ A. J. Cohen, P. Mori-Sánchez, and W. Yang, *Science* **321**, 792 (2008).
¹⁵ K. R. Bryenton, A. A. Adeleke, S. G. Dale, and E. R. Johnson, *Wiley Interdiscip. Rev. Comput. Mol. Sci.*, e1631 (2022).
¹⁶ L. Sham and M. Schlüter, *Physical Review B* **32**, 3883 (1985).
¹⁷ J. P. Perdew, *International Journal of Quantum Chemistry* **28**, 497 (1985).
¹⁸ A. J. Cohen, P. Mori-Sánchez, and W. Yang, *Physical Review B* **77**, 115123 (2008).
¹⁹ A. D. Becke, *J. Chem. Phys.* **119**, 2972 (2003).

- ²⁰ A. D. Becke, *J. Chem. Phys.* **122**, 064101 (2005).
- ²¹ H. Chermette, I. Ciofini, F. Mariotti, and C. Daul, *The Journal of Chemical Physics* **114**, 1447 (2001).
- ²² J. Hostaš, K. O. Pérez-Becerra, P. Calaminici, L. Barrios-Herrera, M. P. Lourenço, A. Tchagang, D. R. Salahub, and A. M. Köster, *The Journal of Chemical Physics* **159** (2023).
- ²³ K. Burke, M. Ernzerhof, and J. P. Perdew, *Chemical Physics Letters* **265**, 115 (1997).
- ²⁴ A. D. Becke, *J. Chem. Phys.* **98**, 5648 (1993).
- ²⁵ C. Adamo and V. Barone, *J. Chem. Phys.* **110**, 6158 (1999).
- ²⁶ M. Ernzerhof and G. E. Scuseria, *J. Comp. Phys.* **110**, 5029 (1999).
- ²⁷ K. R. Brorsen, Y. Yang, M. V. Pak, and S. Hammes-Schiffer, *The journal of physical chemistry letters* **8**, 2076 (2017).
- ²⁸ D. C. Langreth and J. P. Perdew, *Solid State Communications* **17**, 1425 (1975).
- ²⁹ T. Gould and S. G. Dale, *Physical Chemistry Chemical Physics* **24**, 6398 (2022).
- ³⁰ A. J. Price, A. Otero-de-la Roza, and E. R. Johnson, *Chemical Science* **14**, 1252 (2023).
- ³¹ A. J. Price, R. A. Mayo, A. Otero-de-la Roza, and E. R. Johnson, *CrystEngComm* **25**, 953 (2023).
- ³² A. Nandy, D. B. Chu, D. R. Harper, C. Duan, N. Arunachalam, Y. Cytter, and H. J. Kulik, *Physical Chemistry Chemical Physics* **22**, 19326 (2020).
- ³³ Q. Zhao and H. J. Kulik, *The journal of physical chemistry letters* **10**, 5090 (2019).
- ³⁴ J. Yang, S. Falletta, and A. Pasquarello, *npj Computational Materials* **9**, 108 (2023).
- ³⁵ M. Friede, S. Ehlert, S. Grimme, and J.-M. Mewes, *Journal of Chemical Theory and Computation* **19**, 8097 (2023).
- ³⁶ M. Rupp, A. Tkatchenko, K.-R. Müller, and O. A. von Lilienfeld, *Phys. Rev. Lett.* **108**, 058301 (2012).
- ³⁷ B. Huang and O. A. von Lilienfeld, **121**, 10001 (2021).
- ³⁸ D. Khan, S. Heinen, and O. A. von Lilienfeld, *The Journal of Chemical Physics* **159**, 034106 (2023), https://pubs.aip.org/aip/jcp/article-pdf/doi/10.1063/5.0152215/18048072/034106_1_5.0152215.pdf.
- ³⁹ F. Brockherde, L. Vogt, L. Li, M. E. Tuckerman, K. Burke, and K.-R. Müller, *Nature Communications* **8** (2017), 10.1038/s41467-017-00839-3.
- ⁴⁰ S. Dick and M. Fernandez-Serra, *Nature communications* **11**, 3509 (2020).
- ⁴¹ R. Nagai, R. Akashi, and O. Sugino, *npj Computational Materials* **6**, 43 (2020).
- ⁴² J. Kirkpatrick, B. McMorrow, D. H. Turban, A. L. Gaunt, J. S. Spencer, A. G. Matthews, A. Obika, L. Thiry, M. Fortunato, D. Pfau, *et al.*, *Science* **374**, 1385 (2021).
- ⁴³ J. T. Margraf and K. Reuter, *Nature Communications* **12** (2021), 10.1038/s41467-020-20471-y.
- ⁴⁴ M. Welborn, L. Cheng, and T. F. Miller III, *Journal of chemical theory and computation* **14**, 4772 (2018).
- ⁴⁵ K. Karandashev and O. A. von Lilienfeld, *The Journal of Chemical Physics* **156** (2022).
- ⁴⁶ R. Ramakrishnan, P. O. Dral, M. Rupp, and O. A. von Lilienfeld, *Journal of Chemical Theory and Computation* **11**, 2087–2096 (2015).
- ⁴⁷ M. Bogojeski, L. Vogt-Maranto, M. E. Tuckerman, K.-R. Müller, and K. Burke, *Nature Communications* **11** (2020), 10.1038/s41467-020-19093-1.
- ⁴⁸ B. Huang and O. A. von Lilienfeld, *Nature chemistry* **12**, 945 (2020).
- ⁴⁹ A. Pribram-Jones, D. A. Gross, and K. Burke, *Annual review of physical chemistry* **66**, 283 (2015).
- ⁵⁰ R. Ramakrishnan, P. O. Dral, M. Rupp, and O. A. von Lilienfeld, *Scientific data* **1**, 1 (2014).
- ⁵¹ L. Ruddigkeit, R. van Deursen, L. Blum, and J.-L. Reymond, **52**, 2684 (2012).
- ⁵² T. Shiozaki, G. Knizia, and H.-J. Werner, *The Journal of Chemical Physics* **134**, 034113 (2011).
- ⁵³ T. Shiozaki and H.-J. Werner, *The Journal of Chemical Physics* **134**, 184104 (2011).
- ⁵⁴ T. Shiozaki and H.-J. Werner, *Molecular Physics* **111**, 607 (2013).
- ⁵⁵ M. Schwilk, D. N. Tahchieva, and O. A. von Lilienfeld, *arXiv preprint arXiv:2004.10600* (2020).
- ⁵⁶ F. Weigend and R. Ahlrichs, *Physical Chemistry Chemical Physics* **7**, 3297 (2005).
- ⁵⁷ B. Huang, O. A. von Lilienfeld, J. T. Krogel, and A. Benali, *Journal of Chemical Theory and Computation* **19**, 1711 (2023).
- ⁵⁸ J. P. Perdew, K. Burke, and M. Ernzerhof, *Phys. Rev. Lett.* **77**, 3865 (1996).
- ⁵⁹ A. D. Becke, *Phys. Rev. A* **38**, 3098 (1988).
- ⁶⁰ C. Lee, W. Yang, and R. G. Parr, *Phys. Rev. B* **37**, 785 (1988).
- ⁶¹ J. W. Furness, A. D. Kaplan, J. Ning, J. P. Perdew, and J. Sun, *The journal of physical chemistry letters* **11**, 8208 (2020).
- ⁶² J. Sun, A. Ruzsinszky, and J. P. Perdew, *Phys. Rev. Lett.* **115**, 036402 (2015).
- ⁶³ Y. Zhao and D. G. Truhlar, *Theoretical chemistry accounts* **120**, 215 (2008).
- ⁶⁴ J.-D. Chai and M. Head-Gordon, *The Journal of chemical physics* **128** (2008).
- ⁶⁵ G. Montavon, M. Rupp, V. Gobre, A. Vazquez-Mayagoitia, K. Hansen, A. Tkatchenko, K.-R. Müller, and O. A. von Lilienfeld, *New Journal of Physics* **15**, 095003 (2013).
- ⁶⁶ L. Hedin, *Physical Review* **139**, A796 (1965).
- ⁶⁷ F. A. Faber, L. Hutchison, B. Huang, J. Gilmer, S. S. Schoenholz, G. E. Dahl, O. Vinyals, S. Kearnes, P. F. Riley, and O. A. von Lilienfeld, *Journal of Chemical Theory and Computation* **13**, 5255 (2017), PMID: 28926232, <https://doi.org/10.1021/acs.jctc.7b00577>.
- ⁶⁸ Q. Sun, T. C. Berkelbach, N. S. Blunt, G. H. Booth, S. Guo, Z. Li, J. Liu, J. D. McClain, E. R. Sayfutyarova,

- S. Sharma, *et al.*, Wiley Interdisciplinary Reviews: Computational Molecular Science **8**, e1340 (2018).
- ⁶⁹ A. L. Hickey and C. N. Rowley, The Journal of Physical Chemistry A **118**, 3678 (2014).
- ⁷⁰ D. Hait and M. Head-Gordon, Journal of chemical theory and computation **14**, 1969 (2018).
- ⁷¹ A. Tkatchenko, R. A. DiStasio Jr., R. Car, and M. Scheffler, Phys. Rev. Lett. **108**, 236402 (2012).
- ⁷² E. R. Johnson, in *Non-covalent Interactions in Quantum Chemistry and Physics*, edited by A. Otero-de-la-Roza and G. A. DiLabio (Elsevier, 2017) Chap. 5, pp. 169–194.
- ⁷³ S. Grimme, J. Antony, S. Ehrlich, and H. Krieg, J. Chem. Phys. **132**, 154104 (2010).
- ⁷⁴ P. O. Dral, O. A. von Lilienfeld, and W. Thiel, Journal of Chemical Theory and Computation **11**, 2120 (2015), pMID: 26146493, <http://dx.doi.org/10.1021/acs.jctc.5b00141>.
- ⁷⁵ J. J. Kranz, M. Kubillus, R. Ramakrishnan, O. A. von Lilienfeld, and M. Elstner, Journal of chemical theory and computation **14**, 2341 (2018).
- ⁷⁶ M. Stöhr, L. Medrano Sandonas, and A. Tkatchenko, The Journal of Physical Chemistry Letters **11**, 6835 (2020).
- ⁷⁷ C.-W. Ju, E. J. French, N. Geva, A. W. Kohn, and Z. Lin, The Journal of Physical Chemistry Letters **12**, 9516 (2021).
- ⁷⁸ C.-W. Ju, Y. Shen, E. J. French, J. Yi, H. Bi, A. Tian, and Z. Lin, The Journal of Physical Chemistry A (2023).
- ⁷⁹ V. K. Prasad, A. Otero-de-la Roza, and G. diLabio, Machine Learning: Science and Technology **5**, 015035 (2024).
- ⁸⁰ G. Csányi, T. Albaret, M. C. Payne, and A. D. Vita, Phys. Rev. Lett. **93**, 175503 (2004).
- ⁸¹ J. P. Perdew, M. Ernzerhof, and K. Burke, The Journal of chemical physics **105**, 9982 (1996).
- ⁸² J. Čížek, The Journal of Chemical Physics **45**, 4256 (1966).
- ⁸³ J. Čížek and J. Paldus, International Journal of Quantum Chemistry **5**, 359 (1971).
- ⁸⁴ K. Raghavachari, G. W. Trucks, J. A. Pople, and M. Head-Gordon, Chemical Physics Letters **157**, 479 (1989).
- ⁸⁵ G. E. Scuseria and T. J. Lee, The Journal of chemical physics **93**, 5851 (1990).
- ⁸⁶ H.-J. Werner and P. J. Knowles, The Journal of chemical physics **89**, 5803 (1988).
- ⁸⁷ P. J. Knowles and H.-J. Werner, Chemical Physics Letters **145**, 514 (1988).
- ⁸⁸ R. A. Kendall, T. H. Dunning Jr, and R. J. Harrison, The Journal of chemical physics **96**, 6796 (1992).
- ⁸⁹ Q. Sun, X. Zhang, S. Banerjee, P. Bao, M. Barbry, N. S. Blunt, N. A. Bogdanov, G. H. Booth, J. Chen, Z.-H. Cui, *et al.*, The Journal of chemical physics **153** (2020).
- ⁹⁰ Q. Sun, Journal of computational chemistry **36**, 1664 (2015).
- ⁹¹ K. Chen, C. Kunkel, B. Cheng, K. Reuter, and J. T. Margraf, Chemical Science **14**, 4913 (2023).
- ⁹² E. Cignoni, D. Suman, J. Nigam, L. Cupellini, B. Mennucci, and M. Ceriotti, “Electronic excited states from physically-constrained machine learning,” (2023), arXiv:2311.00844 [physics.chem-ph].
- ⁹³ V. Vapnik, *The nature of statistical learning theory* (Springer science & business media, 1999).
- ⁹⁴ C. E. Rasmussen *et al.*, *Gaussian processes for machine learning*, Vol. 1 (Springer).
- ⁹⁵ V. L. Deringer, A. P. Bartók, N. Bernstein, D. M. Wilkins, M. Ceriotti, and G. Csányi, Chemical Reviews **121**, 10073 (2021), pMID: 34398616.
- ⁹⁶ S. Heinen, D. Khan, G. F. von Rudorff, K. Karandashev, D. J. A. Arrieta, A. J. Price, S. Nandi, A. Bhowmik, K. Hermansson, and O. A. von Lilienfeld, arXiv preprint arXiv:2308.11196 (2023).
- ⁹⁷ S. Lee, S. Heinen, D. Khan, and O. A. von Lilienfeld, arXiv preprint arXiv:2308.00389 (2023).
- ⁹⁸ A. S. Christensen, L. A. Bratholm, F. A. Faber, and O. Anatole von Lilienfeld, The Journal of Chemical Physics **152**, 044107 (2020), <https://doi.org/10.1063/1.5126701>.
- ⁹⁹ E. Cignoni, D. Suman, J. Nigam, L. Cupellini, B. Mennucci, and M. Ceriotti, arXiv preprint arXiv:2311.00844 (2023).
- ¹⁰⁰ J. Behler and M. Parrinello, Phys. Rev. Lett. **98**, 146401 (2007).
- ¹⁰¹ K. Hansen, F. Biegler, R. Ramakrishnan, W. Pronobis, O. A. Von Lilienfeld, K.-R. Muller, and A. Tkatchenko, The journal of physical chemistry letters **6**, 2326 (2015).

V. SUPPLEMENTAL MATERIAL

Level of Theory	MAE HOMO [eV]	MAE LUMO [eV]
M06-2X	1.033	0.726
aPBE0 (ML)	1.181	0.764
ω B97XD	0.522	1.491
B3LYP	2.715	0.607
PBE0	2.342	1.182
r ² SCAN	3.474	0.958
PBE	3.738	1.267
BLYP	3.856	1.216

Table IV. HOMO and LUMO eigenvalue errors (eV) compared to GW eigenvalues for 100 molecules from the QM7b dataset⁶⁵. aPBE0 (ML) uses the HF exchange fraction predicted by our ML model trained on the 1169 QM9 atoms from Ref⁵⁷

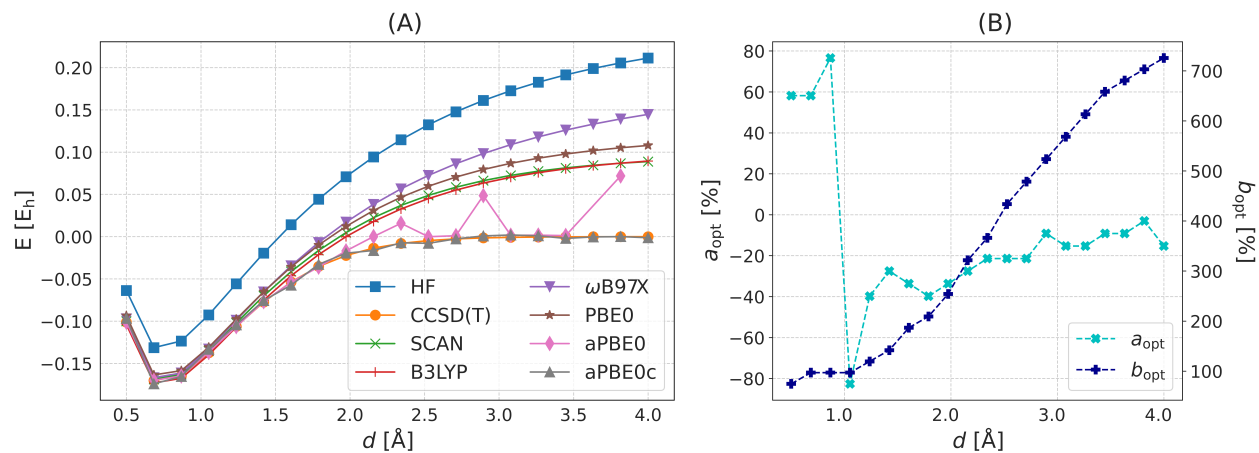


Figure 7. (A) Dissociation energies of H_2 for various level of theories using the cc-pVTZ basis set. (B) a_{opt} and b_{opt} correspond to optimal admixture of exact exchange or PBE correlation in the aPBE0 and aPBE0c functionals respectively.

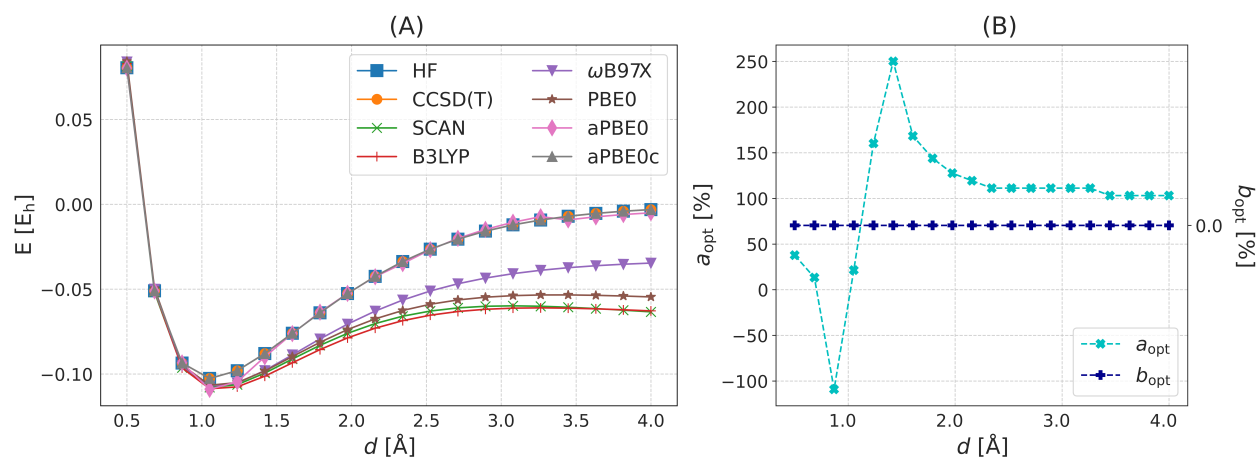


Figure 8. (A) Dissociation energies of H_2^+ for various level of theories using the cc-pVTZ basis set. (B) a_{opt} and b_{opt} correspond to optimal admixture of exact exchange or PBE correlation in the aPBE0 and aPBE0c functionals respectively.

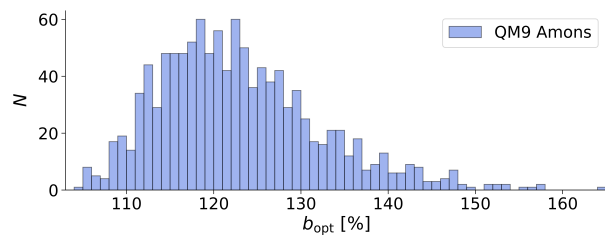


Figure 9. Optimal PBE correlation ratios, b_{opt} , to be employed in the aPBE0c functional for the 1169 QM9 amons⁴⁸ from Ref⁶⁷.

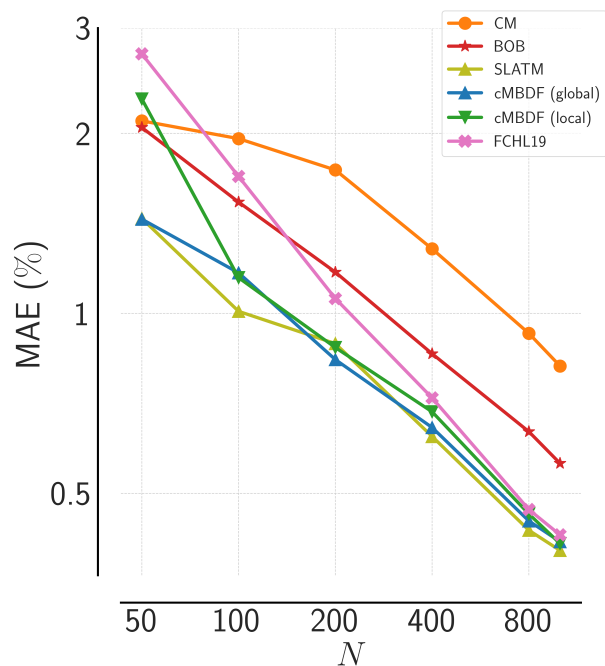


Figure 10. Learning curves showing prediction error for optimal HF admixture ratio ($a_{\text{opt}}^{\text{est}}$) as a function of training set size for the representations Coulomb Matrix (CM)³⁶, Bag of Bonds (BOB)¹⁰¹, Spectrum of London and Axilrod-Teller-Muto potentials (SLATM)⁴⁸, Faber-Christensen-Huang-Lilienfeld 19 (FCHL19)⁹⁸ and convolutional Many Body Distribution Functionals (cMBDF)³⁸. Training and testing (200 out-of-sample atoms) is performed on the set of 1169 atoms from Ref.⁵⁷. It should be noted that training and prediction of the $a_{\text{opt}}^{\text{est}}$ label is surprisingly easier than properties such as energy with simple methods such as CM also showing a very small offset.

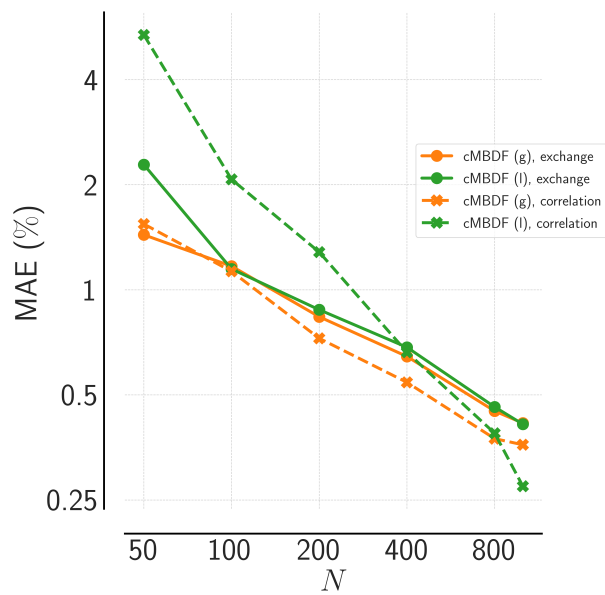


Figure 11. Learning curves showing prediction error for optimal HF admixture ratio ($a_{\text{opt}}^{\text{est}}$) and PBE correlation ratio ($b_{\text{opt}}^{\text{est}}$) as a function of training set size using the convolutional Many Body Distribution Functionals (cMBDF) global (cMBDF(g)) and local (cMBDF(l)) representations³⁸. Training and testing (200 out-of-sample amons) is performed on the set of 1169 amons from Ref.⁵⁷.

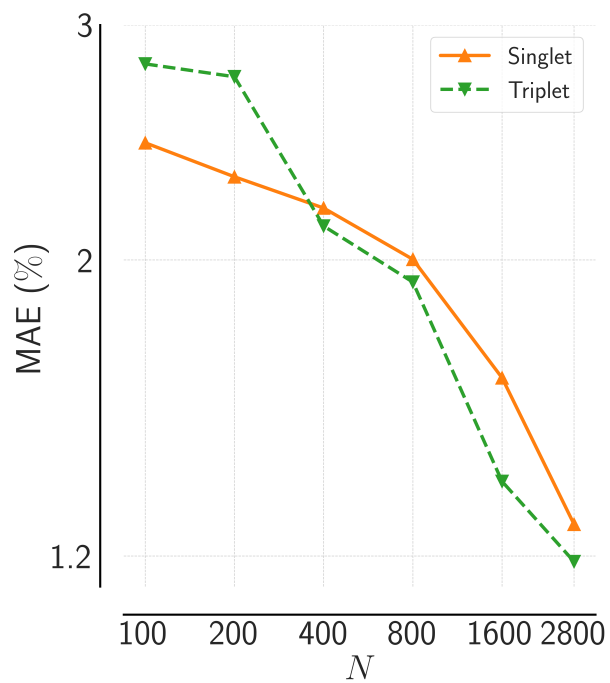


Figure 12. Learning curves showing prediction error for optimal HF admixture ratio ($a_{\text{opt}}^{\text{est}}$) as a function of training set size for carbenes in singlet and triplet states from the QMspin⁵⁵ dataset using the convolutional Many Body Distribution Functionals (cMBDF)³⁸ representation.